Simulating Fracture in Anisotropic Materials Containing Impurities
Supplemental Material

Avirup Mandal
avirupmandal@ee.iitb.ac.in
IIT Bombay
India

Parag Chaudhuri
paragc@cse.iitb.ac.in
IIT Bombay
India

Subhasis Chaudhuri
sc@ee.iitb.ac.in
IIT Bombay
India

1 REFORMULATION OF FRACTURE STRAIN ENERGY DENSITY

We present two different approaches to reformulating strain energy density for a fractured mesh.

1.1 First Approach

Our first approach is based on linearization of the hyper-elastic strain energy first and then projecting out stresses along the fractured edges; and finally weakening just the fractured edges similar to [Khodabakhshi et al. 2016]. The residual stress continues working on the remaining intact edges. The fracture simulation results using this approach are presented in Figure 1.
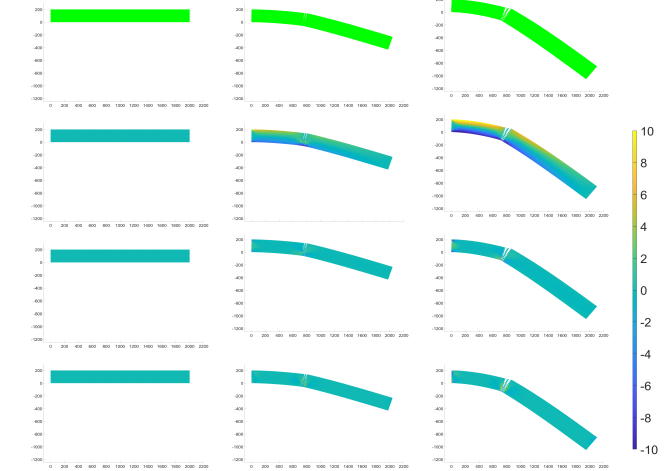
1.2 Second Approach

Our second approach is based on monotonic degradation of strain energy density across all edges similar to the method we have presented in the main paper. The fracture simulation results using this approach are illustrated in Figure 2.

From Figure 1 and Figure 2, we can see that there is no significant change in the visual output of the fracture simulation regardless of the reformulation method used.

2 EDGE LENGTH DEPENDENCE OF ANISOTROPIC ENERGY

Here we prove that the anisotropic strain energy can be represented as a function of edge lengths of the simulation mesh. We begin by briefly reproducing Theorem 2.1 from [Mandal et al. 2021], for completeness.

Table 1 defines some of the symbols frequently used in FEM analysis. These are used in the theorems proved below.

Figure 1: Strain energy density for fracture simulation on a 2**D bar (**1st **row) when only fractured edges are weakened. The corresponding strain profiles are shown in** $2^{nd}(\sigma_x)$, $3^{rd}(\sigma_{xy})$ **and** $4^{th}(\sigma_y)$ **row respectively.**

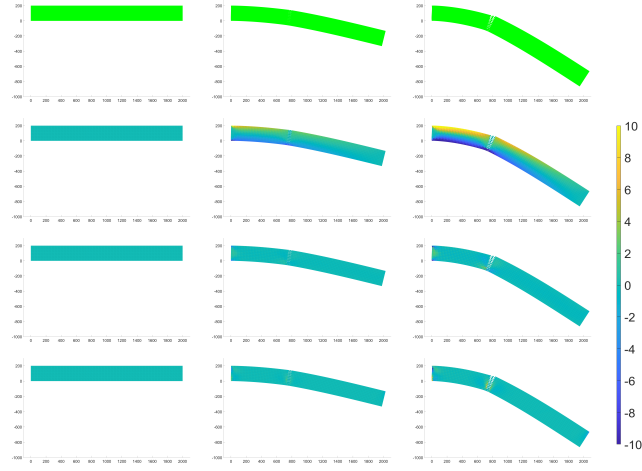| Symbol	Definition
$\mathbf{F} = \mathbf{I} + \nabla_\xi \mathbf{u}$	Deformation gradient
$J = \sqrt{\det(\mathbf{C})}$	Relative volume change
$\mathbf{C} = \mathbf{F}^T\mathbf{F}$	Right Cauchy-Green tensor
$I_C = \text{trace}(\mathbf{C})$	First Right Cauchy-Green invariant
$II_C = \mathbf{C} : \mathbf{C}$	Second Right Cauchy-Green invariant
$III_C = \det(\mathbf{C})$	Third Right Cauchy-Green invariant

Table 1: Quantities frequently used in FEM

THEOREM 2.1. *Every element of the set of invariants* $\mathbf{I}_V = \{I_C, II_C, III_C, IV_C, V_C\}$ *can be expressed in closed form using only the length of the edges of a mesh used in FEM.*

PROOF. Let λ_{ij} be the stretch ratio of an edge formed by nodes i and j in an element Δ_e of FEM mesh which is embedded inside a k-dimensional space.

$$\lambda_{ij}^2 = \left(\frac{d_{ij}^e}{D_{ij}^e}\right)^2 \tag{1}$$

Figure 2: Degradation of hyper-elastic strain energy density for fracture simulation on a 2D bar (1st row). The corresponding strain profiles are shown in 2nd (σ_x), 3rd (σ_{xy}) and 4th (σ_y) row respectively.

where d_{ij}^e and D_{ij}^e denote current and initial length of the edge respectively. It can be shown [Mandal et al. 2021] that

$$\lambda_{ij}^2 = \mathbf{C} \cdot \left(\mathbf{q}_{ij}^e \otimes \mathbf{q}_{ij}^e\right) = \mathbf{C} \cdot \mathbf{Q}_{ij}^e \tag{2}$$

where $\otimes$ denotes tensor product and $\mathbf{Q}_{ij}^e \in \mathbb{R}^{k \times k}$.

$$\mathbf{q}_{ij}^e = \begin{bmatrix} \hat{\mathbf{d}}_{ij}^e \cdot \hat{\mathbf{i}}_1 & \hat{\mathbf{d}}_{ij}^e \cdot \hat{\mathbf{i}}_2 & \dots & \hat{\mathbf{d}}_{ij}^e \cdot \hat{\mathbf{i}}_k \end{bmatrix}^T \tag{3}$$

where $\{\hat{\mathbf{i}}_1, \hat{\mathbf{i}}_2 \dots \hat{\mathbf{i}}_k\}$ denotes a set of orthogonal basis vectors of the k-dimensional space.

Extending this formulation to all the edges (let l) of mesh, we get

$$\mathbf{\Lambda} = \mathbf{C} \cdot \mathbf{Q} \tag{4}$$

where $\mathbf{\Lambda} \in \mathbb{R}^l$ and $\mathbf{Q} \in \mathbb{R}^{k \times k \times l}$, whose entries are equal to λ_{ij}^2 and $\mathbf{Q}_{ij}^e$ respectively.

Finally, the author derived $\mathbf{C}$ by solving an optimization problem

$$\mathcal{L} = \underset{\hat{\mathbf{C}}}{\text{argmin}} \quad ||\hat{\mathbf{C}} \cdot \mathbf{Q} - \mathbf{\Lambda}||_2^2 \tag{5}$$

$$\hat{\mathbf{C}} = \mathbf{\Lambda} \cdot [\mathbf{Q} \otimes \mathbf{Q}]^{\dagger} \cdot \mathbf{Q} \tag{6}$$

where $\dagger$ denotes pseudo-inverse. $\qquad \square$

A more detailed proof of the Theorem 2.1 is available in [Mandal et al. 2021]. However, the anisotropic energy we use in Equation 7 contains a new invariant I_4 which is not based on right Cauchy-Green deformation tensor $\mathbf{C}$, but on the stretch matrix $\mathbf{S}$.

$$\mathbf{\Psi}_{AA}^e = \frac{\mu}{2} \left(\sqrt{I_5} - \Pi(I_4)\right)^2 \tag{7}$$

However, Theorem 2.1 deals only with $\mathbf{C}$-based invariants. Thus arguments presented in Theorem 2.1 are not sufficient for incorporating the anisotropic invariant I_4 and the anisotropic strain energy density, $\mathbf{\Psi}_{AA}^e$. Therefore, next we derive $\mathbf{S}$ in terms of the length of the edges of a mesh used in FEM simulation.

Theorem 2.2. *The anisotropic invariant I_4 can be expressed in closed form using only the length of the edges of a mesh used in FEM.*

Proof. Let us define stretch ratio of an edge, $\tilde{\lambda}_{ij}$, formed by node m and n of an element Δ_e of FEM mesh as

$$\tilde{\lambda}_{ij} = \frac{|d_{ij}^e|}{|D_{ij}^e|} \tag{8}$$

where d_{ij}^e and D_{ij}^e denote current and initial length of the edge respectively.

Using similar arguments as presented in Theorem 2.1, we can now write

$$\tilde{\lambda}_{ij} = \mathbf{S} \cdot \mathbf{O}_{ij}^e = \mathbf{S} \cdot \left(\mathbf{Q}_{ij}^e\right)^{\circ \frac{1}{2}} \tag{9}$$

where $\{.\}^{\circ \frac{1}{2}}$ denotes element-wise square root (Hadamard product) matrix $\mathbf{Q}_{ij}^e$.

Following the same steps as shown in [Mandal et al. 2021] for Theorem 2.1, it is easy to derive the final answer as

$$\mathcal{L} = \underset{\hat{\mathbf{S}}}{\text{argmin}} \quad ||\hat{\mathbf{S}} \cdot \mathbf{O} - \tilde{\mathbf{\Lambda}}||^2 \tag{10}$$

$$\hat{\mathbf{S}} = \tilde{\mathbf{\Lambda}} \cdot [\mathbf{O} \otimes \mathbf{O}]^{\dagger} \cdot \mathbf{Y} \tag{11}$$
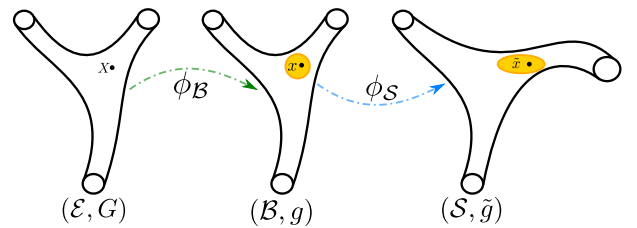
As I_4 is a function of $\mathbf{S}$, it can be concluded that I_4 can also be expressed in closed form using only the length of the edges. This concludes the proof. $\qquad \square$

Thus it is also proved that anisotropic strain energy, $\mathbf{\Psi}_{AA}^e$, which consists of a $\mathbf{S}$-based invariant, I_4, and a $\mathbf{C}$-based invariant, I_5, depends only on the length of the edges of the FEM mesh.

3 GEOMETRIC INTERPRETATION OF EDGE-BASED DAMAGE

The theorems proved in Section 2 together give a geometric interpretation of any hyper-elastic strain energy in terms of the edge length for an undamaged mesh. However, they do not adequately explore the geometric interpretation of edge-based fracture that occurs in graph-based FEM.

To this end, we present a novel theoretical approach to represent any kind of material damage with an appropriate metric embedded in a Riemannian manifold.

Figure 3: Geometric description of the damage (shown in yellow) and deformation as two smooth mappings from Euclidean to Riemannian manifold.

Let us assume that the initial undeformed configuration of a tetrahedral mesh is embedded in a Euclidean manifold $\mathcal{E}$. As shown in Figure 3, the fracture/damage of a mesh without deformation

can be interpreted as a smooth map, $\phi_{\mathcal{B}}$, from Euclidean manifold $\mathcal{E}$ to Riemannian manifold $\mathcal{B}$ [Rastiello et al. 2018] [Das et al. 2021] with corresponding Euclidean metric G and Riemannian metric g [Yavari and Goriely 2012] [Yavari and Marsden 2012]. The deformation of the fractured/damaged mesh can then be interpreted as another smooth map, $\phi_{\mathcal{S}}$, from Riemannian manifold $\mathcal{B}$ to another Riemannian manifold $\mathcal{S}$ with an associated metric $\tilde{g}$ for later.

$$\phi_{\mathcal{B}} : \mathcal{E} \longrightarrow \mathcal{B}$$
$$\phi_{\mathcal{S}} : \mathcal{B} \longrightarrow \mathcal{S} \tag{12}$$

The corresponding deformation gradients are the tangent map of $\phi_{\mathcal{B}}$ & $\phi_{\mathcal{S}}$, and are denoted by a linear map as

$$\mathbf{F}_{\mathcal{B}} : T_X\mathcal{E} \longrightarrow T_x\mathcal{B} \quad \forall X \in \mathcal{E}, \; \forall x \in \mathcal{B}$$
$$\mathbf{F}_{\mathcal{S}} : T_x\mathcal{B} \longrightarrow T_{\tilde{x}}\mathcal{S} \quad \forall x \in \mathcal{B}, \; \forall \tilde{x} \in \mathcal{S} \tag{13}$$

Assuming $\phi_{\mathcal{B}}$ is an identity map, the final deformation gradient from undeformed and undamaged Euclidean manifold to deformed and damaged Riemannian manifold is given by

$$\mathbf{F} = \mathbf{F}_{\mathcal{S}}\mathbf{F}_{\mathcal{B}} = \mathbf{F}_{\mathcal{S}} \tag{14}$$

In this formulation, dislocations are represented by the evolving geometry of the material manifold which is captured by the metric $\tilde{g}$. The transpose of the deformation gradient is defined as

$$\mathbf{F}_{\mathcal{S}}^T : T_{\tilde{x}}\mathcal{S} \longrightarrow T_x\mathcal{B} \quad \forall x \in \mathcal{B}, \; \forall \tilde{x} \in \mathcal{S} \tag{15}$$

Finally, pulled back to the undeformed and undamaged configuration in the Euclidean manifold, the right Cauchy-Green deformation tensor for the deformed and damaged configuration in the Riemannian manifold can be represented as

$$\mathbf{C} : T_X\mathcal{E} \longrightarrow T_X\mathcal{E}$$
$$\mathbf{C} = \mathbf{F}_{\mathcal{S}}^T\tilde{g}\mathbf{F}_{\mathcal{S}} = \mathbf{F}^T\tilde{g}\mathbf{F} \tag{16}$$

Interested readers may check [Yavari and Goriely 2012] [Yavari and Marsden 2012] for a more detailed and rigorous analysis of the geometric representation of deformation and damage.

Analytically defining the Riemann metric $\tilde{g}$ for complex fracture manifold is extremely difficult. However, in our case we can incorporate the effect of the Riemann metric $\tilde{g}$ in Theorem 2.1 and Theorem 2.2 by redefining the stretch ratio (Equation 1 and Equation 8) of an edge as

$$\lambda_{ij}^2 = I_{ij} \left[\frac{d_{ij}^e - d_{ij}^{e^p}}{D_{ij}^e} \right]^2 + \kappa_e \left(1 - I_{ij}\right) \left[\frac{d_{ij}^e}{D_{ij}^e} \right]^2$$

$$\tilde{\lambda}_{ij} = I_{ij} \frac{|d_{ij}^e - d_{ij}^{e^p}|}{|D_{ij}^e|} + \kappa_e \left(1 - I_{ij}\right) \frac{|d_{ij}^e|}{|D_{ij}^e|} \tag{17}$$

$$I_{ij} = \begin{cases} 1 & \text{damaged edge} \\ 0 & \text{undamaged edge} \end{cases}$$

where $d_{ij}^{e^p}$ denote the length of crack opening on the edge between nodes i and j due to fracture. The parameter κ_e is similar to $f(\Phi_l)$ from Equation 18 which denotes the percentage of damage in Δ_e.

hyper

$$\Psi_{frac}^e = f(\Phi_l)\Psi_{ori}^e$$

$$= \left[\frac{|\sigma_{12}^{e'}| + |\sigma_{13}^{e'}| + |\sigma_{14}^{e'}| + |\sigma_{23}^{e'}| + |\sigma_{24}^{e'}| + |\sigma_{34}^{e'}|}{|\sigma_{12}^{e}| + |\sigma_{13}^{e}| + |\sigma_{14}^{e}| + |\sigma_{23}^{e}| + |\sigma_{24}^{e}| + |\sigma_{34}^{e}|} \right] \Psi_{ori}^e \tag{18}$$

The parameter $f(\Phi_l)$ denotes the ratio of total edge stress after and before fracture. Parameters Ψ_{ori}^e and Ψ_{frac}^e denote hyper-elastic strain energy density before and after fracture. Here $\{\sigma_{12}^e \ldots \sigma_{34}^e\}$ and $\{\sigma_{12}^{e'} \ldots \sigma_{34}^{e'}\}$ are the components of normal stress tensor along the direction of the edges before and after fracture respectively.

The rest of the derivations for Theorem 2.1 and Theorem 2.2 remain the same. The Riemann metric $\tilde{g}$ due to fracture can then be obtained by solving $\hat{\mathbf{C}}$ from Equation 6 and $\hat{\mathbf{S}}$ from Equation 11 together.

4 SIMULATION PARAMETERS

Simulation parameters for all our experiments are given in Table 2.

5 PLASTICITY

We use a multiplicative plasticity model [Bargteil et al. 2007] for our work. The deformation gradient is split into an elastic and a plastic part

$$\mathbf{F} = \mathbf{F}_e\mathbf{F}_p \tag{19}$$

The volume of the element is preserved by forcing $\det\left(\mathbf{F}_p\right) = 1$. The plastic part of the deformation gradient, $\mathbf{F}_p$, is updated as follows

$$\mathbf{F}_p \longleftarrow \mathbf{F}_p \cdot \mathbf{V}\left(\det\left(\Sigma\right)^{-\frac{1}{3}}\Sigma\right)^\gamma \mathbf{V}^T \tag{20}$$

where $\mathbf{U}\Sigma\mathbf{V}^T$ is SVD of $\mathbf{F}_e$. The exponent γ is an function of current stress (σ^e), yield stress (σ_{th}^e), flow rate (v) and hardening parameter (α, K)

$$\gamma = \text{clamp}\left\{ \frac{v\left(||\sigma^e||_2 - \sigma_{th}^e - K\alpha\right)}{||\sigma^e||_2}, 0 \ldots 1 \right\} \tag{21}$$

where v and K are user-defined parameters. The term $K\alpha$ controls the work hardening or softening. The term α is initialized with value zero and incremented in each time step by $\alpha \longleftarrow \alpha + \Delta t ||\sigma^e||_2$.

6 EFFECT OF THE RANDOM GRAPH

Figure 4: Effect of using the random graph can be seen here. The impurity map is shown first. A simulated fracture pattern with (middle) and without (right) random graph formulation is shown next.

The random graph-based implementation is crucial to simulating materials with impurities and for artist control of fracture. In order to show this, we simulate a slab that is hinged at one end and which has a band of Gaussian noise impurity in the middle. We tear the slab by pulling it from its free end. We first simulate fracture with our random graph formulation (Figure 4 middle) and then run the

Simulation	# Tetrahedra	sec/frame	Timestep (sec)	Density	Y (Mpa)	ν
Meat Filled Loaf (Meat)	620.5k	4.57	5.0e-03	1.0e+03	1.0e+09	0.4
Meat Filled Loaf (Bread)	620.5k	4.57	5.0e-03	1.0e+03	1.0e+07	0.35
Steak	186.1k	1.33	5.0e-03	1.0e+03	1.0e+09	0.4
Dry Wooden Log	142.5k	1.09	5.0e-03	1.0e+03	1.0e+10	0.45
Wet Wooden log	142.5k	1.18	5.0e-03	1.0e+03	1.0e+10	0.45
Pizza	106.6k	0.81	5.0e-03	1.0e+03	1.0e+07	0.4
Pure Gold Bar	83.8k	0.67	5.0e-03	1.0e+03	1.0e+08	0.2
Gold-Copper Alloy Bar	83.8k	0.73	5.0e-03	1.0e+03	1.0e+08	0.2
Porcelain Column	40.3k	0.31	5.0e-03	1.0e+03	1.0e+10	0.47
Slab (isotropic)	84.3k	0.61	5.0e-03	1.0e+03	1.0e+08	0.45
Slab (anisotropic)	84.3k	0.65	5.0e-03	1.0e+03	1.0e+08	0.45
Slab (with impurities)	84.3k	0.70	5.0e-03	1.0e+03	1.0e+08	0.45
Tube	103.1k	0.78	5.0e-03	1.0e+03	1.0e+08	0.4

Table 2: Simulation parameter table. Parameters Y and *ν* denote Young modulus and Poisson's ratio.

same simulation without it (Figure 4 right). It can be seen from the figure when the random graph formulation is not used, the model disintegration is more chaotic, does not follow the impurity distribution closely and intricate debris pattern disappears.

REFERENCES

Adam W. Bargteil, Chris Wojtan, Jessica K. Hodgins, and Greg Turk. 2007. A Finite Element Method for Animating Large Viscoplastic Flow. *ACM Trans. Graph.* 26, 3 (July 2007), 16–es.

Sanhita Das, Shubham Sharma, Ananth Ramaswamy, Debasish Roy, and J. N. Reddy. 2021. A Geometrically Inspired Model for Brittle Damage in Compressible Elastomers. *Journal of Applied Mechanics* 88, 8 (04 2021). 081002.

Parisa Khodabakhshi, J. N. Reddy, and Arun Srinivasa. 2016. GraFEA: a graph-based finite element approach for the study of damage and fracture in brittle materials. *Meccanica* 51 (2016), 3129 – 3147.

Avirup Mandal, Parag Chaudhuri, and Subhasis Chaudhuri. 2021. Remeshing-Free Graph-Based Finite Element Method for Ductile and Brittle Fracture. *CoRR* abs/2103.14870 (2021). arXiv:2103.14870 https://arxiv.org/abs/2103.14870

Giuseppe Rastiello, Cédric Giry, Fabrice Gatuingt, and Rodrigue Desmorat. 2018. From diffuse damage to strain localization from an Eikonal Non-Local (ENL) Continuum Damage model with evolving internal length. *Computer Methods in Applied Mechanics and Engineering* 331 (2018), 650–674.

Arash Yavari and Alain Goriely. 2012. Riemann–Cartan Geometry of Nonlinear Dislocation Mechanics. *Archive for Rational Mechanics and Analysis* 205 (2012), 59–118.

Arash Yavari and Jerrold E. Marsden. 2012. Covariantization of nonlinear elasticity. *Zeitschrift für angewandte Mathematik und Physik* 63 (2012), 921–927.